Numerical Methods in Civil Engineering

Finding the design collapse capacity of a multi-story RC frame in near-fault based on the collapse risk by using the ratio method

Homa Shanesazzadeh*, Mohsen Tehranizadeh** and Leila Haj Najafi***

Abstract:

The collapse risk role has increasingly drawn engineers' attention in the performance-based design field and engineers tend to design the structures in a way to be qualified enough to resist earthquakes, especially at near-fault sites. Due to specific characteristics of near-fault records, structures in near-fault required more collapse capacity in comparison with far-fault sites. Furthermore, it is necessary to determine the collapse capacity that structures should be designed to comply with standards and to meet the collapse risk limit in the given site. In this research, the ratio method is presented to determine the design collapse capacity of structures based on the risk value of 1% in 50 years as well as the site hazard stemming from the integration scenario for near-fault. In this method, the structure behavior and fundamental period are incorporated, and effect of pulse period is considered as well. This method utilizes the ratio of the collapse capacity of the structure in near-fault to that of far-fault named γ. Consequently, efficient procedures based on nonlinear static pushover are used for obtaining the collapse capacity in far-fault and near-fault. Then, the ratio method is employed on a mid-rise RC frame and the design collapse capacities are acquired for two amounts of Tp/T. The result shows ratio method can be used for any Tp/T values especially those corresponding to the governing Tp at site. Moreover, the least value of γ can be used conservatively since the design collapse capacity of the structure in near-fault is raised by reducing γ.

1. Introduction

The use of risk-based decision-making is on the rise [1]. In earthquake engineering, collapse risk includes the two main components of site hazard and collapse capacity of the structure [2]. Using these components in the risk integral derives the collapse risk. Site hazard is defined by methods such as probabilistic seismic hazard analysis (PSHA) which can be used by integration scenarios for near-fault sites [3]. determine this value in accordance with the risk criterion.

* Ph.D. Candidate, Department of Civil Engineering, Amirkabir University of Technology, Tehran, P.O. Box 15875-4413. Contact info: Tel:+989131155943, Email: homashanehsaz@aut.ac.ir, homa_shanehsaz@yahoo.com.

** Corresponding author: Professor, Department of Civil Engineering, Amirkabir University of Technology, Tehran, P.O. Box 15875-4413, Iran, Tel: 9802164543030, Fax: 9802164543037, Email: dtehz@yahoo.com. tehranizadeh@aut.ac.ir

*** Assistant Professor, Islamic Azad University, Tehran South Branch, Faculty of Engineering, Department of Civil and Environmental Engineering. P.O. Box: 15847-43311, Contact info: Tel: 989122049302, Email: l_najafi@azad.ac.ir.

That is to say, building codes [4,5] have recommended risk limit of 1% in 50 years, so the designed building shall provide the corresponding required collapse capacity in the given site to meet the risk limit.

On the other hand, many prominent cities are located near fault lines; however, there is a lack of knowledge about the characteristics of near-field earthquakes as well as their influence on collapse. The early arriving large amplitude tow-sided pulse in the velocity record, mostly in the normal fault component, is the most significant characteristic of near-fault records which makes them distinguished from ordinary earthquake records. In fact, when the rupture propagation velocity is high enough to be near shear wave velocity, it causes constructive interference of the wavefront and arrives a large amount of energy as a considerable pulse in the time history. This phenomenon usually is called directivity and pulses can be mentioned as directivity pulses [6,7]. The distance to the fault and the magnitude of the earthquake highly affect the occurrence of these pulses. It

has been observed that at distance further than 15 km from the fault, the pulse records are unlikely. An example of pulse-like records is brought in Figure 1 from L'Aquila earthquake in Italy (2009). Baker's algorithm based on the wavelet method [6] is employed to extract the aforementioned velocity pulse along with a circular diagram for the associated score assigned to each direction of the record. The score shows how much of this pulse feature is observable in different directions [6-9].
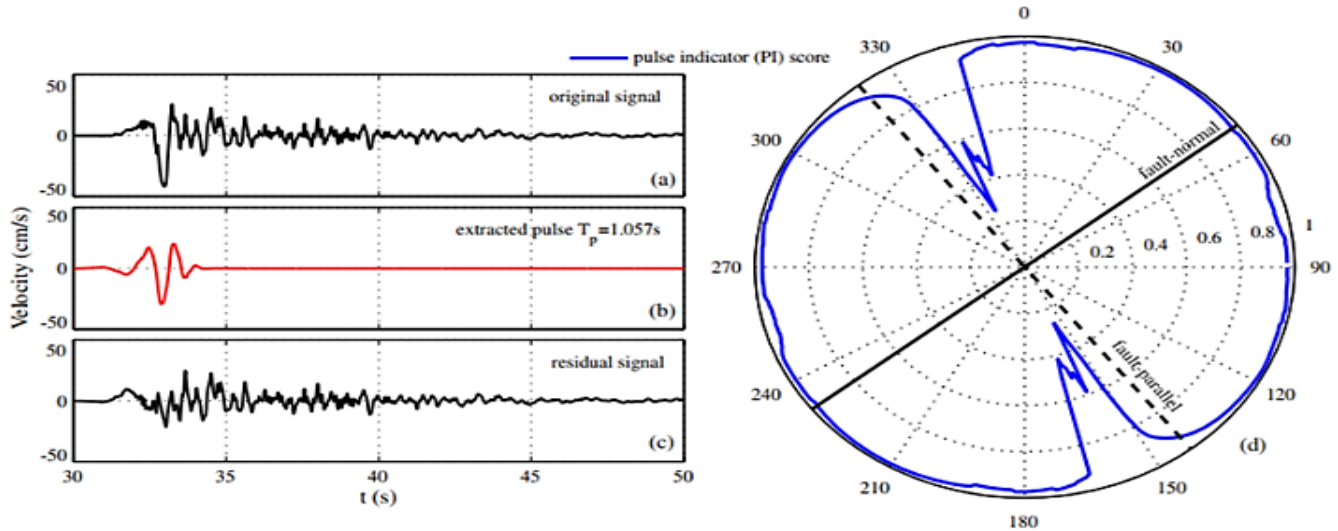

Fig. 1: (a) Original velocity time-history of the Valle Aterno–Centro Valle recording (fault-normal component) from the 2009 M6.3 L'Aquila earthquake (Italy), (b) velocity pulse with pulse period Tp extracted by the methodology in [6], (c) residual velocity signal after extraction of the aforementioned pulse, and (d) polar plot of pulse indicator score per azimuth for all horizontal orientations of the same ground motion.

Due to particular specifications of near-fault pulse-like records, as mentioned above, more attention is needed in this field because buildings subject to these records experience more damage. On the same token, quantifying the impact of near-fault pulses on building seismic collapse using incremental dynamic analysis (IDA) was investigated by Champion and Liel [10].

However, Vamvatsikos and Cornell [11] conducted numerous IDA analyses using ordinary earthquake records to evaluate structures with trilinear backbones. Their findings indicate that the fragility resulting from IDA is related to the parameters of the backbone. Accordingly, the collapse capacity of the structure was determined as a function of the ductility of the structure and the period of its first mode [11].

Furthermore, the nonlinear static procedure method has been utilized increasingly in earthquake engineering performance-based design and modern building codes [4,5]. At first, this procedure was applied for bilinear elastic-perfectly-plastic oscillators and then Baltzopolous et al. developed it for near-fault conditions [12]. Afterward, they extend this procedure to quantify the collapse capacity of the single-degree-of-freedom system with a more comprehend trilinear backbone (Fig. 1) for both near-fault and far-fault conditions [13,14]. Using 130 near-fault pulse-like records, Baltzopoulos et al. [14] reconciled the procedure for near-fault conditions and derived collapse capacity relationships as a function of the pulse period and first mode period. Considering that incremental analysis requires a great deal of computation and is complicated especially for pulse-like records, the mentioned expeditious nonlinear static method has been found more practical to obtain the collapse probability and will be used in this study. It is worth mentioning that in this method, a collapse point occurs when the slope of the IDA diagrams reaches a constant value [14,15].
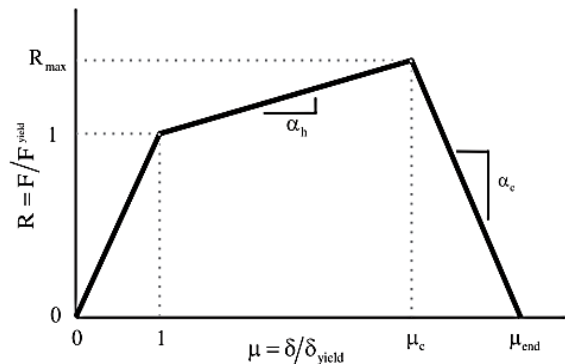

Fig. 1: Representation of trilinear backbone curve in normalized coordinates (ductility μ in the abscissa and reduction factor R in the ordinate) and defining parameters: post-yield hardening slope αh, softening branch negative slope αc, and capping ductility [14].

In this study, we have considered a 12-story mid-rise RC frame designed in accordance with ACI-318 [16] and ASCE7-16 [4], which is located in Tabriz. Yousefi and Taghikhani tracked the seismicity parameters for Tabriz city (Ss=1.458 g and S1=0.81 g) [17]. Based on the 2800 standard code [18], the soil type was determined as type I. The designed frame is subjected to pushover analysis. The simulation of the onset of collapse in static pushover analysis takes into account the nonlinearity of material and

geometric features. After the response curve is determined, the collapse probability distribution is obtained using SPO2IDA in far-fault. Next, collapse probability distributions for pulse periods are calculated using the Baltzopolous et al. method in near-fault. The following sections provide a thorough discussion of the results and related comparisons.

Finally, the ratio method, the ratio of the collapse capacity in near-fault to that of far-fault, will be presented and applied to the above-mentioned frame building to calculate the required collapse capacity of the building in the given site in order to reach the risk value of the standards which is 1% in 50 years. In fact, for this purpose, the collapse capacity which is demanded in accordance with the site hazard and building specifications (building behavior response from static pushover) can be calculated for near-fault and based on the pulse period and fundamental period of the building. This can be called the design collapse capacity because the structure needs to be designed based on this value to meet the risk criteria of the standards.

2. Methodology

Hazard integration scenario in near-fault includes two main parts of pulse-like (near-fault) and without pulse (far-fault) as illustrated in the following equation:

$$\lambda(S_a > x) = \lambda(S_a > x | \text{ no pulse}) + \lambda(S_a > x | \text{ pulse}) \quad (1)$$

where $\lambda(S_a > x)$ is hazard or annual exceedance probability of spectral acceleration, S_a.

The collapse risk value ($P[\text{collapse}]$) is calculated through the integral risk by site hazard ($\lambda(S_a > x)$) and collapse probability ($p[\text{collapse}|S_a]$) as explained in equation (2). Collapse conditional probability, or briefly collapse probability, is defined as the probability distribution for S_a. It shows the probability of collapse conditioned different values of S_a 3and is explained by the fragility curve. The median value of S_a in the fragility curve, which is stemmed from IDAs, presents the collapse capacity [20-22].

$$P[\text{collapse}] = \int p[\text{collapse}|S_a] \lambda(S_a) \, dS_a \quad (2)$$

Based on the previous research [3] and ASCE7-16 [4] the risk value from equation (2) shall be limited to 1% in 50 years for the MCE level. Therefore, equation (3) is obtained using equations (1) and (2) as below:

$$
P[\text{collapse}] = \\
\int p[\text{collapse}|S_a, \text{no pulse}] \lambda(S_a | \text{ no pulse}) \, dS_a \\
+ \int p[\text{collapse}|S_a, \text{pulse}] \lambda(S_a | \text{ pulse}) \, dS_a
\quad (3)
$$

As mentioned above, $\lambda(S_a | \text{ pulse})$ and $\lambda(S_a | \text{ no pulse})$ can be calculated from the hazard integration scenario. In addition, the left side of equation (3) is kept as it is recommended by

research and standards. Hence, the collapse probability in the condition of no pulse $p[\text{collapse}|S_a, \text{no pulse}]$, and also collapse probability in the condition of pulse-like $p[\text{collapse}|S_a, \text{pulse}]$ need to be calculated. Thus, for the given structure located in the given site, the structure needs to be designed so as it will comply with the capacity function of $p[\text{collapse}|S_a, \text{pulse}]$. In this way, the structure has the required design capacity in case of pulse-like occurrences which makes it meet the risk limit. It is worth mentioning since the near-fault records are usually known by their pulse characteristic which distinguishes them from far-fault ones, the pulse-like condition will be referred to as near-fault and no pulse condition will be referred to as far-fault in this study.

As a result, $p[\text{collapse}|S_a, \text{no pulse}]$ and $p[\text{collapse}|S_a, \text{pulse}]$ are the only unknown values in equation (3) which are needed to be calculated. Hereafter, the ratio method is presented to solve the equation and find the values of $p[\text{collapse}|S_a, \text{no pulse}]$ and $p[\text{collapse}|S_a, \text{pulse}]$. If the ratio of the collapse capacity in the near-fault to that of the far-fault can be estimated, we can have the design collapse capacity in the near-fault $p[\text{collapse}|S_a, \text{pulse}]$ as the only unknown value to calculate and put the value of the far fault capacity as a coefficient of the near-fault collapse capacity. Therefore, equation (3) can be solvable by the only unknown value of the design near-fault capacity. By calculating the near-fault collapse capacity required based on the site hazard and risk value, the design far-fault collapse capacity can be found by the considered ratio or coefficient.

Consequently, the ratio of the collapse capacity in the near-fault to that of the far-fault is the key factor to find the required capacity of the structure based on the given site hazard and the risk limit. The ratio depends on the structure's dynamic behavior and specifications. As a matter of fact, the most effective parameters are the fundamental period and ductility of the structure which is implied by the behavior diagram of the structure, trilinear type in this study, as illustrated in Fig. **1** [14]. Moreover, the ratio of the pulse period to the fundamental period of the structure (Tp/T) is another effective parameter in finding the collapse capacity in the near-fault condition [21].

In accordance with the above-mentioned, in this study, the ratio method will be gone through and applied to the RC frame. For this purpose, the collapse capacity of the structure will be calculated in near-fault as well as far-fault. The collapse capacity in near-fault will be discussed for different ratios of the Tp/T for the given structure. Finally, the required value of the collapse capacity for the structure will be found utilizing equation (3) based on the risk limit and site hazard and ratio method. It is worth mentioning that since the ratio method depends on the Tp/T and behavior of

the structure, these parameters are included in the final result.

To clarify the whole process, the following items outline the steps that will be followed:

1. Designing and modeling the structure, and employing the pushover analysis
2. Utilizing simplified methods based on the pushover results to determine the structure collapse capacity in far-fault and near-fault
3. Using the ratio of the collapse capacity in near-fault to that of far-fault from the last step in addition to equation (3) to find the design collapse capacity.

In the next part, the method for estimating the collapse capacity of the structure in near-fault and far-fault will be described as it will be used in the ratio method.

3. Design and modeling

A 12-story mid-rise RC special moment frame designed according to the ASCE7-16 [4] and ACI 318-2019 [5] is used with the ratio method here. The considered special moment frame is loaded as a perimeter frame system of a symmetric plan (the space frames of the building are assumed as the simple frames sustaining the majority of the gravity load). The total height (H) of 48 m is designed with an identical span length of 6 m, and 4 m story heights.

Consisting of 3 bays, the model provides the interior and exterior columns and joints [23]. The beam and column sections are identical for every two stories. The designed frame meets the mentioned code seismic provisions, including strong column-weak beam ratios and shear capacity design requirements, serviceability limits, and detailing requirements. The connections of the 1st story columns to the foundation at the ground level are assumed to be fixed, and the soil impacts are negligible. The design spectral acceleration of SDS=0.9 g and SD1= 0.4 g are used according to the ASCE7-16 [4] and seismicity parameters for Tabriz city reported by Taghikhani and Yousefi [17] for the assumed region in Tabriz city. The design specification and details are presented in Tables 1 and 2 for the beam and column sections.

In Table 1 which is allocated to beam specifications, the first column shows the story of the beam. Beam sections describe the dimension of the beam sections which is also addressed by h and b. the No. of transverse bars presents the quantity of rebars used in the section for transverse reinforcement, and ϕt states the diameter of them where s is for their spaces along the component. No. ϕl explains the number of longitudinal rebars and the final column of the table illustrates their diameter. Similar notifications have been used in Table 2, but for column components with square sections.

Table 1: Design specifications and rebar details for beam sections

Story	Beams section	h (m)	b (m)	No. of transverse bars	Shear rebar ϕt (mm)	s (m)	No. ϕl-design at bottom	No. ϕl-design at top	Longitudinal rebar ϕl (mm)
1	90x70	0.9	0.7	3	14	0.15	5	6	28
2	90x70	0.9	0.7	3	14	0.15	5	6	28
3	90x70	0.9	0.7	5	14	0.15	6	7	28
4	90x70	0.9	0.7	5	14	0.15	6	7	28
5	90x70	0.9	0.7	6	14	0.15	7	8	28
6	90x70	0.9	0.7	6	14	0.15	7	8	28
7	80x60	0.8	0.6	4	14	0.15	5	6	28
8	80x60	0.8	0.6	4	14	0.15	5	6	28
9	80x60	0.8	0.6	3	14	0.15	5	6	28
10	80x60	0.8	0.6	3	14	0.15	5	6	28
11	75x60	0.75	0.6	3	14	0.15	3	4	28
12	75x60	0.75	0.6	3	14	0.15	3	4	28

Table 2: Design specifications and rebar details for column sections

Story	Columns section	h (m)	Number of transverse bars	Shear rebar ϕt	s (m)	No. ϕl-design	Longitudinal rebar ϕl (mm)
1	125x36-28	1.25	7	14	0.12	36	28
2	125x36-28	1.25	7	14	0.12	36	28

3	125x28-28	1.25	7	14	0.12	28	28
4	125x28-28	1.25	7	14	0.12	28	28
5	125x36-28	1.25	7	14	0.12	36	28
6	125x36-28	1.25	7	14	0.12	36	28
7	115x32-28	1.15	6	14	0.12	32	28
8	115x32-28	1.15	6	14	0.12	32	28
9	115x28-28	1.15	6	14	0.12	28	28
10	115x28-28	1.15	6	14	0.12	28	28
11	105x28-28	1.05	5	14	0.12	28	28
12	105x28-28	1.05	5	14	0.12	28	28

There is a strong tendency for global collapse to occur through sidesway collapse for most ductile structures as well as a few limited-ductile structures that have a weak or soft story [4, 23]. As a result, collapse assessments are only carried out in this study based on flexural failure modes (i.e. sidesway collapse). Nevertheless, shear failure in beams, columns, and joints is checked to ensure that shear failure is not dominant in the model.

Modeling structure and performing nonlinear static analysis have been conducted with the help of OpenSees [24] computer code by considering of 5% damping ratio for overall models.

The inelastic flexural response of beam-column elements can be modeled using one of the five idealized model types shown in Fig. **2** falling into two main categories: 1) lumped or concentrated plasticity at the ends of the element, or 2) distributed plasticity along the element length [25]. In the lumped plasticity models, the inelastic response is concentrated at the ends of the element (Fig. **2** (a) and Fig. **2** (b)), while in the distributed plasticity models, the inelastic deformations are simulated either in a finite length hinge model (Fig. **2** (c)). Fiber formulation (Fig. **2** (d)) distributes plasticity using numerical integrations through the member cross-sections and along the member length, or finally through the use of the finite element model (Fig. **2** (e)). The finite element model is the most complex and breaks down the continuum along the member length and cross-sections [25].
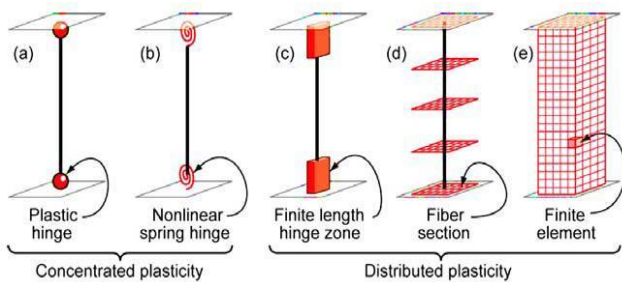

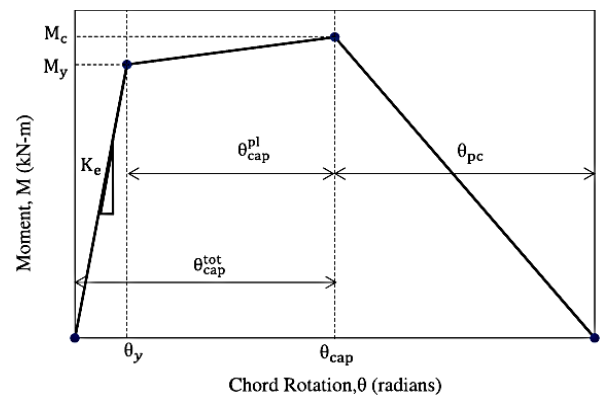**Fig. 2:** Idealized models of beam-column elements [25]

Fig. 3: Monotonic behavior of the component model developed by Ibarra et al.[26]

RC structures are typically modeled using lumped plasticity [21, 27]. The Beam-With-Hinges element, shown in Fig. **2**, contributes to multifaceted and complex models by identifying further modes of failure. A modified Ibarra-Medina-Krawinkler (IMK) deterioration model is used to model the flexural behavior of the material [28]. Fig. **3** illustrates the moment-curvature properties of nonlinear sections in hinges. The hysteretic model developed by Ibarra et al. [26] is chosen since it is capable of simulating the strength and stiffness degradation experienced during seismic collapse. The beam-column joints are modeled rigidly as stated in ASCE41 [29]. The bar-slip effect is incorporated into the model. P-Δ effects are considered in the modeling and analysis through leaning columns along with large deformation geometric transformations.

Based on the empirical equations developed by Haselton et al. [30], the design parameters of an RC element are related to the peak-ordinated hysteresis response. These calibrated equations are according to the modified Ibarra-Medina-Krawinkler (IMK) deterioration models shown in Fig. **2** (b) to simulate the response of 255 rectangular column tests. By using column properties, regression-based equations have been developed to estimate linear and nonlinear parameters as well as in-cycle and cyclic degradation of rotational springs [30, 22]. To obtain the corresponding hinge behavior

values for the IMK model depending on section properties, related equations are used in this study. They are brought as follows [30]:

$$\frac{EI_y}{EI_g} = 0.30 \left(0.1 + \frac{P}{A_g f'_c}\right)^{0.80} \left(\frac{L_s}{h}\right)^{0.72},$$ (4)

where $0.2 \le \frac{EI_y}{EI_g} \le 0.6$

$$\theta_{cap,pl} = 0.12(1 + 0.55a_{sl})(0.16)^v(0.02 + 40\rho_{sh})^{0.43}(0.54)^{0.01c_{unit}f'_c}(0.66)^{0.1S_n}(2.27)^{10.0\rho}$$ (5)

$$v = P / A_g f'_c$$ (6)

$$\theta_{pc} = (0.76)(0.031)^v(0.02 + 40\rho_{sh})^{1.02} \le 0.10$$ (7)

$$M_c/M_y = 1.13$$ (8)

$$\Gamma = (170.7)(0.27)^v(10)^{s/d}$$ (9)

$$\rho_{sh} = \frac{A_{sh}}{sb}$$ (10)

where Ash, s, and b are the total cross-sectional area of transverse reinforcement, the spacing of transverse reinforcement, and the width of columns measured perpendicular to transverse load, respectively. It is worth stating that the average amount of $\frac{M}{M_y} = 1.13$ is suggested by Haselton because this ratio will not significantly change by various values of axial load and rebar ratios [31].

4. Far-fault collapse capacity calculation using SPO2FRAG

This method has been developed based on the relationship between the structures behavior diagram and the collapse capacity of the structure from incremental dynamic analyses. By determining the structure's behavior parameters and using the equivalent single degree of freedom method we can calculate the median (or fractiles of 16, 84 percent) of the collapse probability distribution. Having the median value and standard deviation of 0.6 as well as assuming the lognormal distribution which are both used commonly in standards and research [3, 4] (because the collapse capacity of structure complies with lognormal probability distribution) collapse probability of the structure can be defined.

As shown in Fig. **1**, the structure behavior diagram is defined by three main components which are 1) hardening slop αh 2) softening slope αc 3) the ductility of the peak point μc, other parts of the diagram can be easily driven based on these three components.

Fig. **4** illustrates the verification of this method with IDA results for the given structure behavior diagram [13].
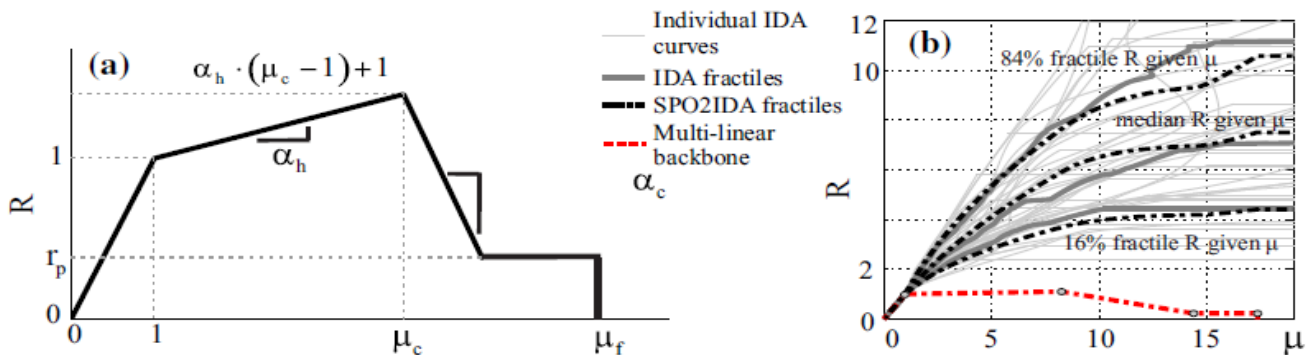

Fig. 4: Verification of SPO2IDA method for the given structural behavior diagram [13].

5. Using the analytical method based on pushover to calculate the collapse capacity in near-fault

Like what has been mentioned in the previous part for far-fault, the procedure for near-fault has been developed by Baltzopoulos et al. [14]. Using the same behavior parameters, the collapse capacity corresponding to each percentile can be calculated with the following equations depending on the Tp/T.

$$R_{cap,x\%} = \left(1 + d_{x\%} \cdot \frac{\mu_c - 1}{\mu_{eq} - 1}\right).$$ (11)

$$\left[R^o_{x\%}(\mu_c) + \mu_{peak} \cdot \exp\left(\frac{a_{x\%} \cdot \ln\mu_{cap(100-x)\%}}{\ln\mu_{cap(100-x)\%} + b_{x\%}}\right)\right],$$

$$x = \{16, 50, 84\}, \quad d_{x\%} = g\left(\mu_{eq}, |\alpha_c|, \frac{T}{Tp}, T\right), \quad a_{x\%},$$

$$b_{x\%} = g\left(|\alpha_c|, \frac{T}{Tp}, T\right)$$

$$R^o_{x\%}(\mu_c) = \widehat{R}_{x\%}(\mu_c) - \mu_{peak} \cdot \exp\left(\frac{a_{x\%} \cdot \ln\mu_c}{\ln\mu_c + b_{x\%}}\right)$$

$\widehat{R}_{x\%}(\mu_c)$ is calculated by replacing μ_c in the following equation and obtaining R.

$$\ln\mu_{x\%}=\frac{a_{x\%}.\ln^2 R +b_{x\%}.\ln R}{c_{x\%}.\ln R+d_{x\%}},\quad a_{x\%},\ b_{x\%},\ c_{x\%}, \tag{12}$$

$$d_{x\%}=g\left(\alpha_h,\frac{T}{T_p},T\right)$$

The coefficients of a, b, c, and d are obtained from function g which is implied in the related MATLAB code. Function g provides these coefficients based on the behavior

parameters, pules period, and fundamental period of the structure.

The verification for this method has been presented in Figure 6 [14]. As the red points show the IDA result, it is observed that the simplified procedure which is shown by continuous line for median and dotted line for one standard deviation less and more, aligned well with IDA results.
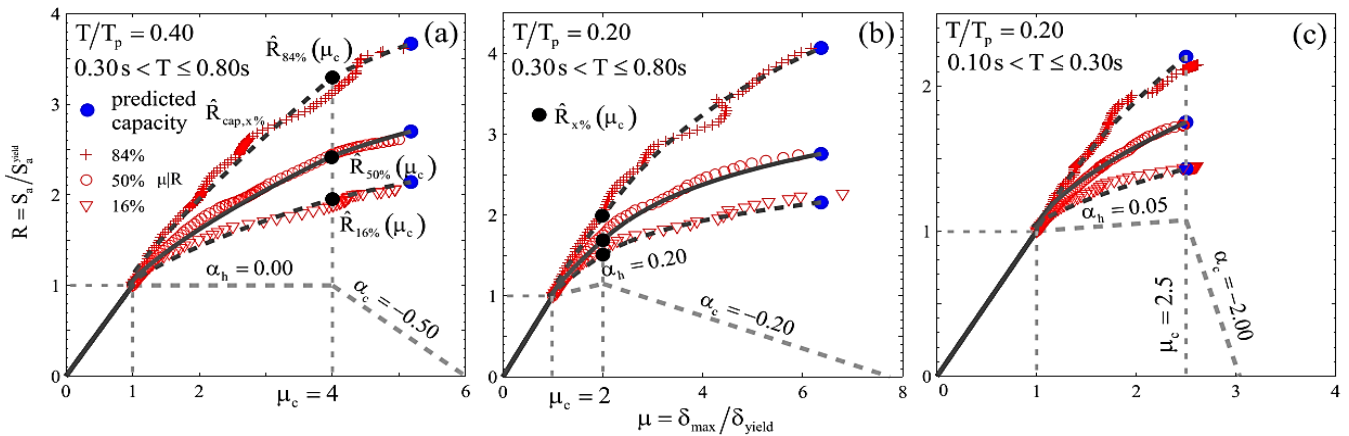

Fig. 6: Verification of analytical method for estimating collapse capacity in near-fault by IDA results [14].

6. Estimation of the hazard curves for near-fault and far-fault conditions

According to the probabilistic seismic hazard analysis developed in [17, 19] with integration scenario for near-fault and far-fault in Tabriz, the location with the least distance to fault has been chosen (3 km). This location has the maximum amplification of near-fault spectral acceleration to and Table 3.

the far-fault corresponding value. The estimated spectral accelerations for 2475 years of return period are 0.74g and 0.63g for near-fault and far-fault, respectively. In addition, for 475 years of the return period, the corresponding values are 0.4 for near-fault and 0.35g for far-fault. Since the hazard curve can be estimated by two given points [32] using equation (13), the related coefficients of the hazard curve (k and k0) are calculated as shown in

$$H(im)=k_0.im^{-k} \tag{13}$$

The corresponding hazard curves for calculated coefficients of near-fault and far-fault conditions have been demonstrated in Fig 7.

Table 3: Finding the coefficients of the hazard curve for near-fault condition

Sa (g)	Return Period (years)	Exceedance Probability in 50 years	Annual Probability of Exceedance		k=	4.855
					-k0=	0.01468
0.74	2475	0.020	0.00040	=	-k0	(e^0.74)^-k
0.4	475	0.100	0.00211	=	-k0	(e^0.4)^-k

Table 3: Finding the coefficients of the hazard curve for far-fault condition

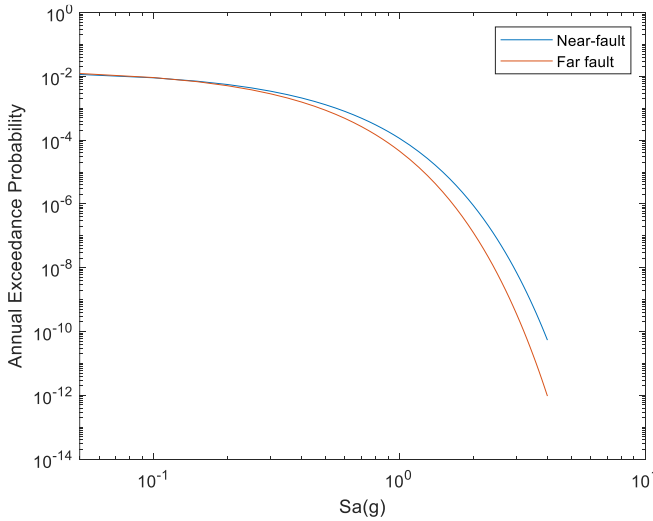| Sa (g)	Return Period (years)	Exceedance Probability in 50 years	Annual Probability of Exceedance		k=	5.895
					-k0=	0.01657
0.63	2475	0.020	0.00040	=	-k0	(e^0.63)^-k
0.35	475	0.100	0.00211	=	-k0	(e^0.35)^-k

Fig 7: Hazard curves for near-fault and far-fault.

7. Using ratio method to find the required collapse capacity based on the collapse risk limit

For the considered case that has been described in the previous part, the fundamental period of the structure is 1.58 sec. Since the frame is symmetric and regular in height the equivalent single degree of freedom method is applicable here. According to the [13], it is assumed that the n-story frame is subject to the lateral load profile of $F_i = K.m_i.\varphi_i$ where Fi is the load and mi is the floor mass for story i. φ_i is the dimensionless displacement profile with unit value at roof. K is the scale factor with dimension of acceleration [13] (Fig. 8).
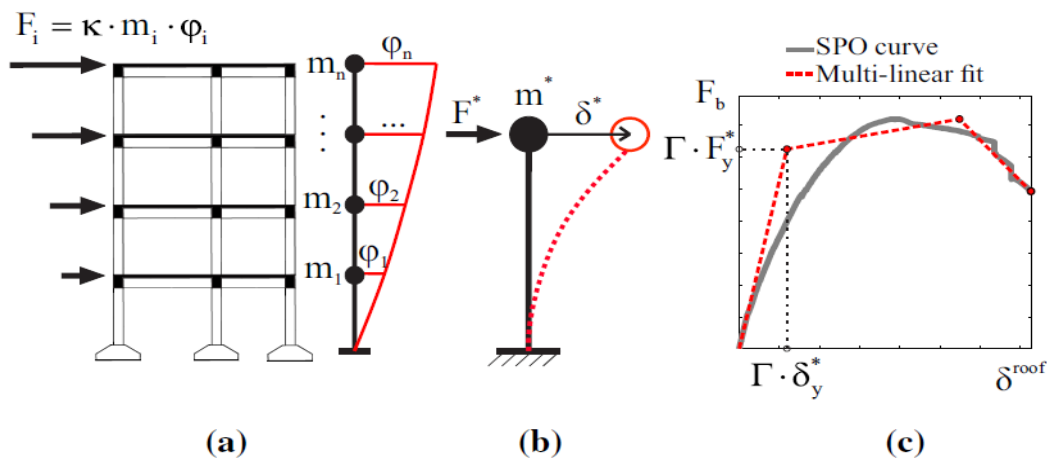

Fig. 8: Definition of equivalent SDOF system: SPO analysis of the structure (a), definition of dynamic characteristics of the SDOF system (b), definition of the monotonic backbone of the SDOF system based on SPO curve (c) [13]

For the equivalent system the corresponding values is calculated as below:

$$m^* = \sum_{i=1}^{n} m_i \varphi_i \tag{14}$$

$$\Gamma = m^* / \sum_{i=1}^{n} m_i \varphi_i^2 \tag{15}$$

$$F^* = F_b / \Gamma \tag{16}$$

$$\delta^* = \delta^{roof} / \Gamma \tag{17}$$

$$T^* = 2\pi \sqrt{m^* \delta_y^* / F_y^*} \tag{18}$$

where Γ is the modal participation factor and T* is the equivalent period which are obtained as Γ =1.323 and T*=1.8 for the case.

The behaviour diagram parameters have been found as follows:

$$\alpha_h = 0.006 \ , \quad \mu_c = 3.89, \quad \alpha_c = 0.138$$

The calculated collapse capacity, utilizing the methods described in the above parts, has been brought in Fig. 9. As expected, the median value of the collapse capacity in near-fault depends on Tp/T, while for near fault a constant value is illustrated at the top of the diagram.
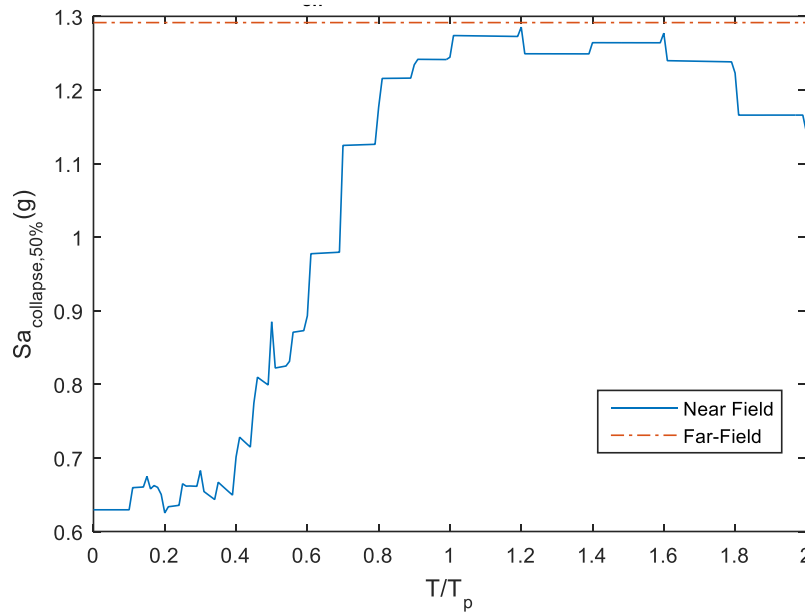
Fig. 9: Median collapse capacity for various T/Tp for the design state superimposed on the far-field result.

For using the ratio method to find the required design collapse capacity in the sites based on the hazard, risk limit and structure specification, the ratio of the median collapse capacity in near-fault to that of far-fault is needed. This ratio is named γ here for brevity. In this study, γ is considered for two states of Tp/T=1 and Tp/T=0.5, but this can be considered for the governing pulse period of the site if it is known for any cases. The obtained values are brought in Table 4 (NF: near-fault, FF: far-fault). It is worth mentioning that the ratio of 0.67 in the following table is close to the corresponding value of 0.7 which is addressed in reference [33] for a structure with the same fundamental period of 1.8 s.

Table 4: The values of γ for the given structure for Tp/T=1 and Tp/T=0.5

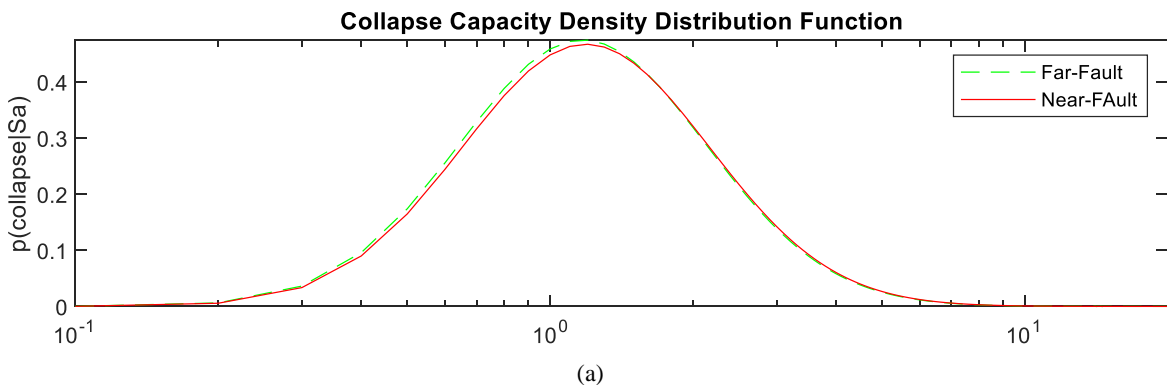|	Sa_Collapse NF/Sa_Collapse FF
Tp/T=1	0.97
Tp/T=0.5	0.67

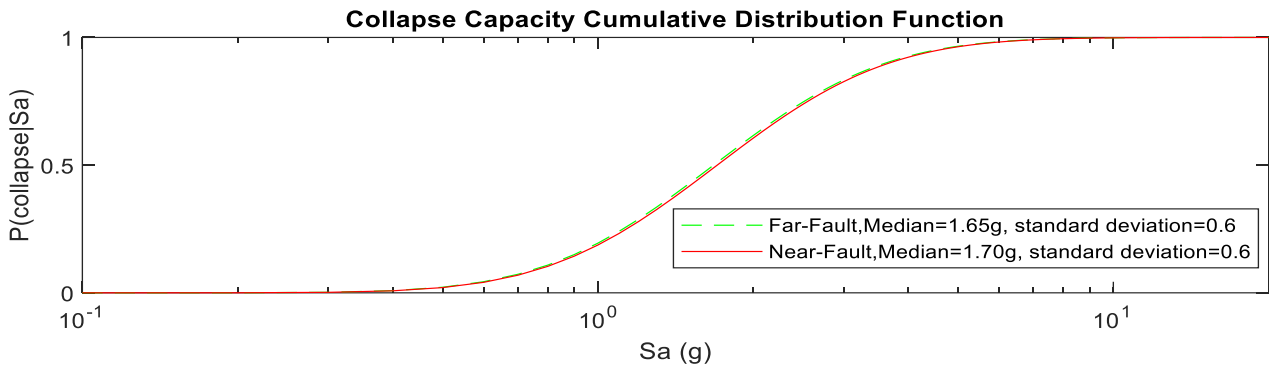In other words, the factor of γ states that if the collapse capacity in far-fault is multiplied by γ, the collapse capacity in near-fault results. Hence, in design, we should increase the capacity of the structure in near-fault by $1/\gamma$ in comparison with far-fault design to make the structure able to resist subject to pulse like near-fault records. This concept is implied in equation (3) using the lognormal distribution and standard deviation of β and then resulted in the following equations:

$$P[collapse] = \int \ln(Sa_{FF}, \beta) \, \lambda(S_a| \text{ no pulse}) \, dS_a +$$
$$\int \ln(Sa_{NF}, \beta) \, \lambda(S_a| \text{ pulse}) \, dS_a \qquad (19)$$

$$P[collapse]$$
$$= \int \ln(Sa_{FF}, \beta) \, \lambda(S_a| \text{ no pulse}) \, dS_a + \int \ln(Sa_{FF}$$
$$/\gamma, \beta) \, \lambda(S_a| \text{ pulse}) \, dS_a \qquad (20)$$

Solving equation (20) is through the try and modification process as there are two functions in each integral and there is not any practical straight solution for that. The process has been developed in a MATLAB code and the results are illustrated in Fig. and Fig. **5** for γ=0.97 and γ=0.67, respectively.

Collapse Capacity Density Distribution Function

(a)

Collapse Capacity Cumulative Distribution Function

(b)

Fig. 10: Results for design collapse capacity calculated for γ=0.97 in density probability function shown in figure (a) and cumulative probability function in figure (b) based on the hazard curves of far-fault and near-fault and 1% collapse risk in 50 years

Collapse Capacity Density Distribution Function

(a)

Collapse Capacity Cumulative Distribution Function
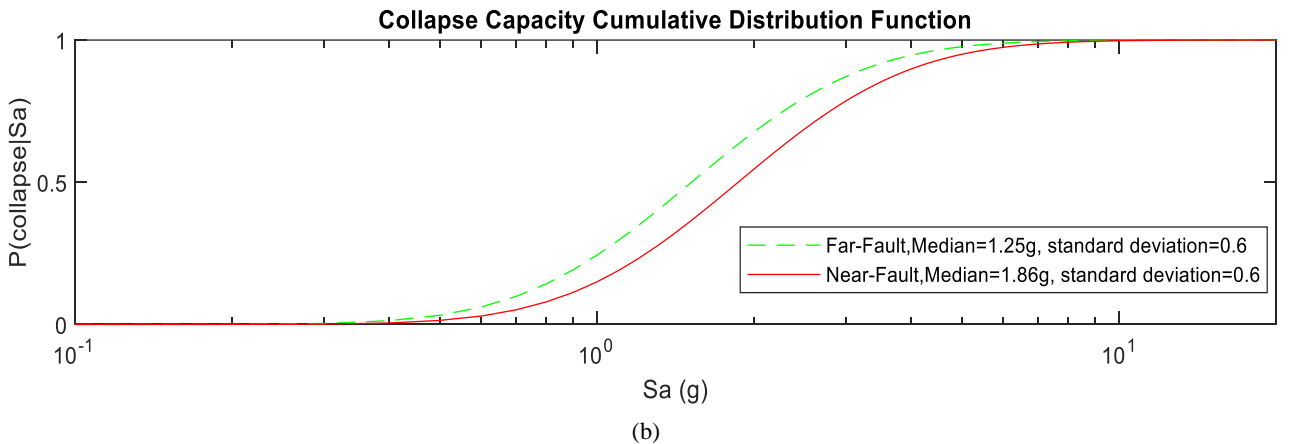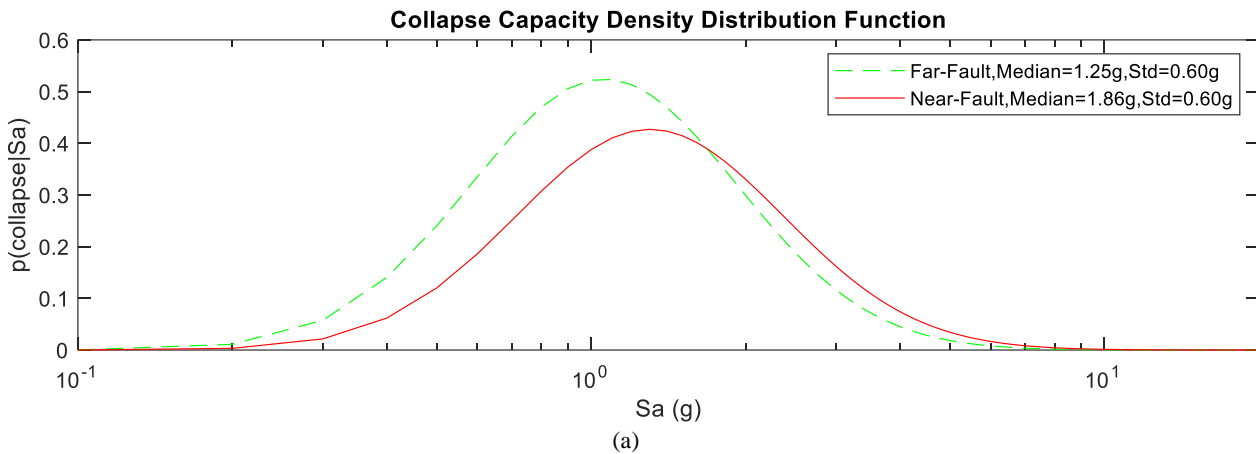
(b)

Fig. 51: Results for design collapse capacity calculated for γ=0.67 in density probability function shown in figure (a) and cumulative probability function in figure (b) based on the hazard curves of far-fault and near-fault and 1% collapse risk in 50 years

The result shows increasing the amount of γ causes a rise in far-fault design capacity but reduces the near-fault design capacity. To put it in another way, since the less value of γ provides a larger design capacity in near-fault, it is conservative to use the least value of γ in the site if we are not sure about adopting the governing value of Tp/T for the site. For instance, in this case, minimum γ is 0.48 and the corresponding values for near-fault and far-fault design capacities are 2.06g and 1g, respectively. It can be observed that with 28% reduction in γ, design capacity in near-fault has risen by 11%.

8. Conclusion

In this study, the ratio method has been presented to find the design collapse capacity in near-fault. In this method, the design collapse capacity of the structure is obtained based on the site hazard and collapse risk limit considering structure specifications including fundamental period and behavior diagram. Furthermore, the pulse period effect is incorporated in this method. As the ratio of the near-fault collapse capacity to the far-fault one, which is called γ, is needed in the presented method, the expeditious procedure

based on nonlinear static pushover of the structure has been utilized to find collapse capacity. Then, the presented ratio method has been applied on an RC frame and design collapse capacities for near-fault have been determined for two cases of Tp/T as well as the minimum amount of γ. Results show that as γ increases the design collapse capacity for near-fault is reduced. Therefore, if the data of the site is not comprehensive to determine the governing pulse period which γ should be considered for, the minimum value of γ can provide the conservative design collapse capacity for near-fault.

References

[1] Ellingwood, B.R. and Wen, Y.-K. (2005), Risk-benefit-based design decisions for low probability-high consequence earthquake events in Mid-America. Prog. Struct. Engng Mater., 7: 56-70. https://doi.org/10.1002/pse.191

[2] Judd, J. and Charney, F. (2014). Earthquake risk analysis of structures in structural dynamics, EURODYN 2014, A. Cunha, et al., Editors, Porto, Portugal, pp. 2929- 2938

[3] Luco, N., Ellingwood, B.R., Hamburger, R.O., Hooper, J.D. Kimball, J.K. and Kircher, C.A. (2007), Risk-Targeted versus Current Seismic Design Maps for the Conterminous United States.

[4] ASCE- Minimum design loads for buildings and other structures (2016), ASCE-SEI 7- 16, American Society of Civil Engineers: Reston, Virginia.

[5] Applied Technology Council, Quantification of building seismic performance factors (2009) (FEMA P695), NEHRP Recommended Provisions for Seismic Design of New Buildings and Other Structures, FEMA P-695, Federal Emergency Management Agency Washington, D.C.

[6] Baker, J.W. (2007). Quantitative classification of near-fault ground motions using wavelet analysis", Bulletin of the Seismological Society of America, 97(5), pp. 1486-1501 26

[7] Baker, J.W. and Cornell, C.A. (2008). Vector-valued intensity measures for pulse-like near-fault ground motions", Engineering Structures, 30(4), pp. 1048-1057

[8] Tehranizadeh, M. and Shanehsazzadeh, H. (2011). Nearfault amplification factor by using wavelet method", Research, Development and Practice in Structural Engineering and Construction. DOI: 10.3850/978- 981-08-7920-4 St-35-0117

[9] Tehranizadeh, M. and Shanehsazzadeh, H. (April 2011). Directivity effects on near-fault amplification factor", Urban Earthquake Engineering, Sharif university.

[10] C. Champion and A. Liel, "The effect of near-fault directivity on building seismic collapse risk," EARTHQUAKE ENGINEERING AND STRUCTURAL DYNAMICS, vol. 41, p. 1391–1409, 2012.

[11] D. Vamvatsikos and C. Cornell, "Direct estimation of seismic demand and capacity of multiple-degree of-freedom systems through incremental dynamic analysis of single degree

of freedom approximation," Journal of Structural Engineering, vol. 131, p. 589–599, 2005 .

[12] G. Baltzopoulos, C. Chioccarelli and I. Iervolino, "The displacement coefficient method in near-source conditions," Earthquake Engineering and Structural Dynamics, vol. 44(7), p. 1015–1033, 2015.

[13] G. Baltzopoulos, R. Baraschino, I. Iervolino and D. Vamvatsikos, "SPO2FRAG: software for seismic fragility assessment," Bull Earthquake Eng, vol. 15, p. 4399–4425, 2017.

[14] G. Baltzopoulos, D. Vamvatsikos and I. Iervolino, "Analytical modeling of near-source pulse-like seismic demand for multi-linear backbone oscillators," EARTHQUAKE ENGINEERING & STRUCTURAL DYNAMICS, 2016 .

[15] D. Vamvatsikos and C. Cornell, "Direct estimation of seismic demand and capacity of multiple-degree of-freedom systems through incremental dynamic analysis of single degree of freedom approximation," Journal of Structural Engineering, vol. 131, p. 589–599, 2005.

[16] Building Code Requirements for Structural Concrete, Institute., American Concrete (ACI 318-19) and Commentary, Farmington Hills, MI, 2019.

[17] Yousefi, M. and Taghikhany, T. (2014). Incorporation of directivity effect in probabilistic seismic hazard analysis and disaggregation of Tabriz city", Natural Hazards. DOI 10.1007/s11069-014-1096-5

[18] "Iranian code of practice for seismic resistant design of buildings", Standard No. 2800, 4th edition (2014)

[19] Shahi, S.K. and Baker, J.W. (2014). An efficient algorithm to identify strong velocity pulses in multi-component ground motions", Bulletin of the Seismological Society of America, 104(5), pp. 2456-2466

[20] M. Kohrangi, M., Bazzurro, P., Vamvatsikos, D., (2021) Seismic risk and loss estimation for the building stock in Isfahan: part II—hazard analysis and risk assessment. Bulletin of Earthquake Engineering. 19, 1739–1763.

[21] Haselton, C.B., Liel, A., Deierlein, G.G., Dean, B.S., and Chou, J.H. (2010). Seismic collapse safety of reinforced concrete buildings. I: Assessment of ductile moment frames", Journal of Structural Engineering, 137(4), pp. 481-491

[22] Liel, A., Haselton, C.B., and Deierlein, G. (2010). Seismic collapse safety of reinforced concrete buildings. II: Comparative assessment of nonductile and ductile moment frames", Journal of Structural Engineering, 137(4), pp. 492-502

[23] Champion, C. and Liel, A. (2012). The effect of near-fault directivity on building seismic collapse risk", Earthquake Engineering & Structural Dynamics, 41(10), pp. 1391- 1409

[24] C. Haselton and G. Deierlein, "Assessing Seismic Collapse Safety of Modern Reinforced Concrete Frame Buildings," Blume Center Technical Report, vol. 156, 2007 .

[25] F. Mckenna, "OpenSees: A Framework for Earthquake Engineering Simulation," vol. 13, no. 4, pp. 58-66, 2011 .

[26] "Seismic performance assessment of buildings" Federal Emergency Management Agency (FEMA), Washington, DC, 2012.

[27] L. Ibarra, R. Medina and H. Krawinkler, "Hysteretic models that incorporate strength and stiffness deterioration," Earthquake Engineering and Structural Dynamics, vol. 34, p. 1489–1511, 2005 .

[28] M. B. Shoraka, T. Y. Yang and K. J. Elwood, "Seismic loss estimation of non-ductile reinforced concrete buildings," Earthquake Engineering & Structural Dynamics, vol. 42, no. 2, pp. 297-310, 2013.

[29] L. F. Ibarra and H. Krawinkler, "Global Collapse oF Frame Structures Under Seismic Excitations," Department of Civil and Environmental Engineering Stanford University, 2005.

[30] Seismic Evaluation and Retrofit of Existing Buildings, American Society of Civil Engineers, ASCE/SEI 41-17, 2017 .

[31] C. B. Haselton, A. Liel, S. Taylor-Lange and G. Deierlein, "Calibration of Model to Simulate Response of Reinforced Concrete Beam-Columns to Collapse," ACI STRUCTURAL JOURNAL, pp. 1141-1152, 2016 .

[32] C. B. Haselton, A. Liel, S. Lange and G. Deierlein, "Beam-Column Element Model Calibrated for Predicting Flexural Response Leading to Global Collapse of RC Frame Buildings," PEER report, 2007.

[33] Lazar, N., and Dolšek, M., (2014). A closed form solution for seismic risk assessment incorporating intensity bounds", Engineering Structures, Elsevier, Vol78, pp. 78-79,

[34] Liel, A., Luco, N., Raghunandan, M., Champion, C., (2015). Modifications to risk-targeted seismic design maps for subduction and near-fault hazards. International Conference on Applications of Statistics and Probability in Civil Engineering, ICASP12 ,Vancouver, Canada, July 12-15.